Trends in Upper-Tropospheric Humidity: Expansion of the Subtropical Dry Zones?

MIRIAM TIVIG[a] AND VERENA GRÜTZUN[b]

Meteorological Institute, Center for Earth System Research and Sustainability (CEN), Department of Earth Sciences, Universität Hamburg, Hamburg, Germany

VIJU O. JOHN

User Service and Climate Division, EUMETSAT, Darmstadt, Germany

STEFAN A. BUEHLER

Meteorological Institute, Center for Earth System Research and Sustainability (CEN), Department of Earth Sciences, Universität Hamburg, Hamburg, Germany

(Manuscript received 16 January 2019, in final form 17 December 2019)

ABSTRACT

Subtropical dry zones, located in the Hadley cells' subsidence regions, strongly influence regional climate as well as outgoing longwave radiation. Changes in these dry zones could have significant impact on surface climate as well as on the atmospheric energy budget. This study investigates the behavior of upper-tropospheric dry zones in a changing climate, using the variable upper-tropospheric humidity (UTH), calculated from climate model experiment output as well as from radiances measured with satellite-based sensors. The global UTH distribution shows that dry zones form a belt in the subtropical winter hemisphere. In the summer hemisphere they concentrate over the eastern ocean basins, where the descent regions of the subtropical anticyclones are located. Recent studies with model and satellite data have found tendencies of increasing dryness at the poleward edges of the subtropical subsidence zones. However, UTH calculated from climate simulations with 25 models from phase 5 of the Coupled Model Intercomparison Project (CMIP5) shows these tendencies only for parts of the winter-hemispheric dry belts. In the summer hemisphere, even though differences exist between the simulations, UTH is increasing in most dry zones, particularly in the South and North Pacific Ocean. None of the summer dry zones is expanding in these simulations. Upper-tropospheric dry zones estimated from observational data do not show any robust signs of change since 1979. Apart from a weak drying tendency at the poleward edge of the southern winter-hemispheric dry belt in infrared measurements, nothing indicates that the subtropical dry belts have expanded poleward.

1. Introduction

The upper-tropospheric humidity distribution plays a major role in the climate system especially in the tropics and subtropics, where it contributes strongly to the water vapor feedback (Held and Soden 2000). This region situated roughly between 30°N and 30°S is characterized by strong contrasts in the upper-tropospheric humidity distribution, with very high humidity in the intertropical convergence zone (ITCZ) and very low humidity in the subtropical dry zones, where the subsidence branches of the Hadley and Walker circulations are located. These dry zones are relevant not only for the surface climate underneath, which is characterized by low precipitation and very dry climatic conditions, but also for the radiative budget, as outgoing longwave radiation is higher in regions where the atmosphere is dry (Pierrehumbert 1995). The logarithmic dependence between water vapor concentration and outgoing longwave radiation leads to higher sensitivity to changes in the dry part of the distribution. Therefore, even

[a] Current affiliation: GEOMAR Helmholtz Centre for Ocean Research Kiel, Kiel, Germany.

[b] This work is dedicated to the memory of Verena Grützun (died 2018), without whose inspiration and contribution to the satellite simulation this project would not have been finished.

Corresponding author: Miriam Tivig, mtivig@geomar.de

DOI: 10.1175/JCLI-D-19-0046.1

small changes in humidity in the upper-tropospheric dry zones can have strong influence on the water vapor feedback (Spencer and Braswell 1997).

Recent model simulations have revealed a widening of the subtropical subsidence zones associated with the weakening and poleward expansion of the Hadley circulation (Lu et al. 2007). Under the influence of increased carbon dioxide (CO_2) concentration, simulations revealed signals of reduced relative humidity at the poleward flanks of the subtropical dry zones as well as further drying inside the dry zones (Lau and Kim 2015; Cai et al. 2012; Roca et al. 2012; Sherwood et al. 2010; Lu et al. 2007). In satellite observations from infrared radiation sounders, subtropical dry zones appear to have expanded poleward by 2°–4.5° over the period 1979–2005 (Hudson et al. 2006; Hu and Fu 2007). Positive trends of upper-tropospheric humidity, however, were identified over monsoon regions, the deep tropics, and the midlatitudes (Gierens et al. 2014; Johanson and Fu. 2009; Hu and Fu 2007; Bates and Jackson 2001).

Some previous studies analyzed the dry zones and their evolution in different seasons. Stephens et al. (1996) studied upper-tropospheric humidity from satellite measurements and were the first to point out that, over the domain of the Hadley circulation, the relative humidity of the upper troposphere undergoes significant seasonal changes. Scheff and Frierson (2012) have looked at humidity in different seasons, but studied precipitation decline instead of upper-tropospheric humidity. Schröder et al. (2014) introduced the frequency of occurrence of dry air in the free troposphere, to study the radiatively sensitive range of the free tropospheric humidity distribution, but calculated from observations only and for a restricted area and time range. In the current study, we therefore analyze upper-tropospheric dry zones from a global view, with respect to seasonality and climate change. To do so, we use a variable that can be retrieved from satellite measurements as well as from model data, in order to make a comparison of the resulting trends more straightforward.

Soden and Bretherton (1993) defined the concept of upper-tropospheric humidity (UTH), as a measure for humidity vertically averaged over a broad layer of the upper troposphere (approximately between 200 and 500 hPa). UTH is calculated from brightness temperatures by a simple transformation relation. This relation can also be adapted to brightness temperatures retrieved from model data through a satellite simulation software. UTH from model data can be directly compared with results of satellite measurements.

The humidity distribution in the upper troposphere and the intertropics reveals that the subsidence zones are changing their features depending on the seasonal shift of the ITCZ. Therefore, it is worth analyzing the upper-tropospheric dry zones separately for the seasons when the ITCZ is in its northernmost [boreal summer; June–August (JJA)] and southernmost [boreal winter; December–February (DJF)] position, respectively.

In the next section we describe the data and method used to derive UTH from model data and from radiances measured from satellite-based sensors. Section 3 explores the trends in dry zones found in the model experiments and in observations since 1979. Section 4 encompasses a discussion of the results and some concluding remarks.

2. Data and methods

a. Model data

To compute UTH, we used the output of 25 models (Table 1) from phase 5 of the Coupled Model Intercomparison Project (CMIP5) (Taylor et al. 2012). First, we analyzed the output of the idealized CMIP "1pctCO2" experiment, in which the atmospheric CO_2 concentration is gradually increased by 1% per year. In this experiment, the CO_2 concentration starts from a preindustrial state and is approximately doubled after 70 and quadrupled after 140 model years.

In a second step we compared the results with the output of the historical simulations of the CMIP5 models. The models simulate the recent past from 1850 to 2000 or later, imposing changing conditions like atmospheric composition due to both anthropogenic and volcanic influences, solar forcing, emissions or concentrations of short-lived species, natural and anthropogenic aerosols, and time-evolving land use (Taylor et al. 2012).

UTH is not a standard humidity variable given by the models but rather is derived from brightness temperatures usually measured by satellite-based sensors. To compute UTH from model data in the same way as from measurements, the output of the models has first to be transformed into radiance, as seen by a satellite sensor. Temperature and humidity profiles as well as the wind fields for surface emissivity are used as input for the fast radiative transfer model for TIROS Operational Vertical Sounder (TOVS) known as RTTOV (Saunders et al. 2010). To be consistent with observations and because brightness temperature measured with microwave sensors are less influenced by clouds, we produced brightness temperatures matching the specifications of channel 18 of the Advanced Microwave Sounding Unit (AMSU-B) (see section 2b). For comparison we also computed brightness temperatures with the specifications of channel 12 of the High Resolution Infrared Radiation Sounder (HIRS).

b. Satellite data

Satellite measurements of brightness temperature used to retrieve UTH are typically made in two specific

TABLE 1. CMIP5 models used for the current study with their respective institute. (Expansions of acronyms are available online at http://www.ametsoc.org/PubsAcronymList.)

Model name	Modeling center or group
ACCESS1.3	Commonwealth Scientific and Industrial Research Organization (CSIRO) and Bureau of Meteorology (BOM), Australia
BCC-CSM1.1 and BCC-CSM1.1(m)	Beijing Climate Center, China Meteorological Administration
CanESM2	Canadian Centre for Climate Modeling and Analysis (CCCMA)
CCSM4	National Center for Atmospheric Research (NCAR)
CESM1(BGC)	Community Earth System Model Contributors
CNRM-CM5 and CNRM-CM5.2	Centre National de Recherches Météorologiques / Centre Européen de Recherche et Formation Avancée en Calcul Scientifique
CSIRO-Mk3.6.0	Commonwealth Scientific and Industrial Research Organization in collaboration with Queensland Climate Change Centre of Excellence
FGOALS-g2	LASG, Institute of Atmospheric Physics, Chinese Academy of Sciences and CESS, Tsinghua University
FGOALS-s2	LASG, Institute of Atmospheric Physics, Chinese Academy of Sciences
GFDL-ESM2G and GFDL-ESM2M	NOAA Geophysical Fluid Dynamics Laboratory
GISS-E2-H	NASA Goddard Institute for Space Studies
HadGEM2-ES	Met Office Hadley Centre and contribution by Instituto Nacional de Pesquisas Espaciais)
IPSL-CM5A-LR, IPSL-CM5A-MR and IPSL-CM5B-LR	Institut Pierre-Simon Laplace
MIROC-ESM	Japan Agency for Marine-Earth Science and Technology, Atmosphere and Ocean Research Institute (The University of Tokyo), and National Institute for Environmental Studies
MIROC5	Atmosphere and Ocean Research Institute (The University of Tokyo), National Institute for Environmental Studies, and Japan Agency for Marine-Earth Science and Technology
MPI-ESM-MR and MPI-ESM-LR	Max-Planck-Institut für Meteorologie (Max Planck Institute for Meteorology)
MRI-CGCM3	Meteorological Research Institute
NorESM1-M and NorESM1-ME	Norwegian Climate Centre

frequency regions: in the infrared at 6.7 μm and in the microwave at 183.31 GHz. Since the end of the 1970s, the HIRS instruments on board of the National Oceanic and Atmospheric Administration (NOAA) operational polar-orbiting satellites have been measuring water vapor radiances using the 6.7-μm infrared channel. In the field of global satellite data analysis this is the only source of data providing such a long time series (Jackson et al. 2003). Over the years, instrument changes have led to intersatellite biases, but efforts have been made during the last two decades to intercalibrate the radiance measurements in order to create a consistent time series of the satellite data (e.g., Bates and Jackson 2001; Shi et al. 2008).

Top of the atmosphere infrared radiance measurements are affected by clouds, which can create errors when retrieving humidity. This additional source of bias has been tackled by restricting the data to clear-sky pixels and homogenizing it (Shi and Bates 2011). In this study, we used the UTH data from Shi and Bates (2011), which were calculated using the Soden and Bretherton (1993) approach including a reference pressure to make them comparable to the microwave UTH from model data (see section 2c). This dataset has a resolution of 2.5° × 2.5°. Unfortunately, UTH datasets generated from clear-sky measurements revealed a dry bias of up to 30% RH or more in convective regions (John et al. 2011). Even though in the present study the focus is on the dry regions, the dry bias is still important with about −9% RH in the tropical UTH values (John et al. 2011). However, the availability of HIRS data since 1979 makes it a valuable source of information with regard to climate evolution.

Microwave sensors are less sensitive to clouds. Datasets of UTH from microwave radiances, even when processed with a cloud filter, show only small biases in convective regions of about 2%–3% RH (John et al. 2011). Therefore, we mainly used UTH computed from radiances measured with the microwave sensor AMSU-B from the satellites *NOAA-15*, *-16*, and *-17* and the Microwave Humidity Sounder from *NOAA-18* and *MetOp-A* [updated version of Chung et al. (2013)]. Data for this study were taken from channel 18 at 183.31 ± 1.00 GHz of the AMSU-B sensor, because the sensitivity of brightness temperature for this frequency to relative change in humidity is highest in the upper troposphere. UTH from microwave data comes on a 1.5° grid. However, microwave data are only available from 1999 to 2018.

c. *The brightness temperature transformation method*

Brightness temperatures originating from model data as well as from measurements of satellite-based sensors are used to calculate UTH. For this purpose, Soden and Bretherton (1993) derived a relation between infrared radiances and upper-tropospheric humidity, which has also been adapted to microwave radiances by Buehler and John (2005):

$$\ln\left[\frac{\mathrm{UTH}}{\cos(\theta)}\right] = a + bT_b, \tag{1}$$

where ln is the natural logarithm, θ is the zenith angle, T_b is radiance expressed in brightness temperature, and a and b are regression coefficients, which were determined for UTH with respect to liquid water. UTH is a weighted mean of the fractional relative humidity in the upper troposphere. The constants depend on the sensor and its viewing angle (Buehler and John 2005). For this study, UTH was calculated for a nadir-viewing sensor; therefore, $\cos(\theta) = 1$. The original relation from Soden and Bretherton (1993) also included a term for the scaled reference pressure p_0 and a dimensionless lapse rate parameter β:

$$\ln\left[\frac{\mathrm{UTH}p_0}{\beta\cos(\theta)}\right] = a + bT_b. \tag{2}$$

Like Buehler and John (2005) we decided to stay with the simpler version of the relationship for the microwave data but use the expression with p_0 for the infrared data. This approach is supported by the study by Lang (2019), which shows that T_b has no explicit emission layer pressure dependence for microwave data but does have one for infrared data, which can be accounted for by p_0. We refer to Jackson and Bates (2001) for the analysis of other variants of UTH calculation. The coefficients used for the current study can be found in Table 2.

TABLE 2. Constant coefficients for calculation of UTH from brightness temperature for a nadir-looking sensor, with regard to liquid water.

Sensor	a	b (K^{-1})
HIRS	31.500	−0.115
AMSU-B	16.474	−0.070

Whereas the infrared-based equation from Soden and Bretherton (1993) to calculate UTH requires brightness temperature from clear-sky conditions, radiance simulated from CMIP5 model data, although ignoring the radiative effect of clouds, reflects all-sky humidity profiles. This leads to a dry bias of the HIRS data discussed in section 2b, which should be small in the dry zones.

d. *Method of trend calculation*

To analyze the change in UTH and especially in the regions with low UTH values, we first calculated trends, using the climate data operator "cdo trend" (Schulzweida 2019), which performs an ordinary least squares linear regression for each grid point of each dataset. As the trends are estimated separately for the two seasons DJF and JJA, the trends in UTH of the corresponding seasonal time series are given in percent RH per time step (month of the corresponding season) and multiplied by the number of months in a decade (30 for the seasonal trends). Then, trends are transformed into percent per decade relative to the mean UTH of the first decade, to make them better comparable between the different datasets. But using relative trends also emphasizes the trends in the dry zones, if the absolute trends are of similar range throughout the distribution.

To evaluate the evolution of dry zones with time, we also calculated for each time step the fraction of grid points where UTH is smaller than a given threshold, depending on the source of the data used to evaluate UTH. The thresholds have been chosen as the upper boundary of the 25th percentile, knowing that the distribution of UTH differs depending on the source of the data (model or observation; microwave or infrared). Tests have shown that, even though the fraction of dry grid points is depending on the given threshold, the trend or evolution of this fraction is similar for thresholds around the selected percentile. One can alternatively use other thresholds, but results in terms of trends do not change very much. The linear trend is again calculated by regression. To be consistent with observations, only the grid points in the tropics and subtropics have been chosen for the model data (between 45°S and 45°N).

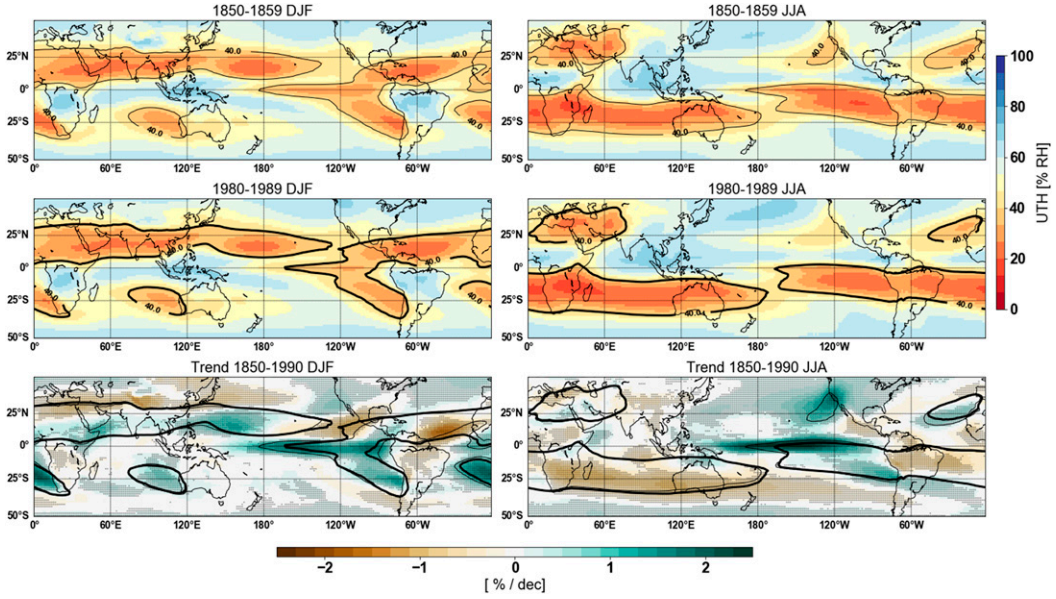

FIG. 1. Decadal ensemble mean of UTH calculated from the output of the 1pctCO2 simulation with 25 CMIP5 models, with the specification of a microwave sensor. Comparison of (top) the first decade 1850–59 and (middle) the last decade 1980–89, and (bottom) the trend in UTH for the whole period relative to the mean UTH of the first decade, for (left) DJF and (right) JJA. The contour lines in the bottom plots indicate the regions with UTH ≤ 40% RH in 1850–59 (thin line) and in 1980–89 (thick line). The black shading indicates grid points with a robust signal (see explanations in the text).

3. Results

a. UTH from CMIP5 models

Figure 1 shows the mean of the first (1850–59, top panels) and the last decade (1980–89, middle panels) of the spatial distribution of UTH calculated from the ensemble mean of the 1pctCO2 simulations, using the microwave sensor algorithm. The UTH distribution is depicted separately for DJF (Fig. 1, left panels) and JJA (Fig. 1, right panels). Because 1pctCO2 is an idealized experiment not taking into account the real climate of the last 150 years, the names of the decades (1850–59 and 1980–89) are not referring to the historical period. The bottom panels of Fig. 1 show the trend per decade, in percent relative to the mean UTH from the first decade, for both seasons respectively. The black contour lines indicate the regions where the ensemble mean of UTH is smaller than 40% RH. Following previous studies like Lau and Kim (2015) we define these regions as the subtropical dry zone. The stippling in the bottom panels indicate grid points, where the sign of the trend in UTH is robust. Robust means here, that at least 68%, or 17 of 25, of the models show the same sign (increasing or decreasing UTH).

The subtropical dry zones behave differently depending on the season. In the winter hemisphere, the dry zones form a belt over the subtropics, whereas in the summer hemisphere the dry zones are mainly located in eastern subtropical ocean basins, corresponding to the descent zones of the subtropical anticyclones. As the distribution of UTH depends on the hemisphere and on the season, the evolution of the dry zones has been considered separately for DJF and JJA, when the ITCZ is in its southernmost and northernmost position, respectively.

In the experiment with gradually increasing CO_2 concentration, two features can be observed considering the evolution of the dry zones (bottom panels of Fig. 1). First, even though the black contour lines (indicating the 40% RH level) only show small shifts between the first and the last decade, a decreasing trend in UTH is nevertheless visible on the poleward edge of the dry belt in the winter hemisphere. This is especially true in DJF over the Mediterranean Sea region and central Asia, and in JJA in the Indian Ocean and southwestern Pacific Ocean. This drying trend could be related to a poleward expansion of subtropical subsidence zones, which has been revealed in recent studies with models and observations (e.g., Birner et al. 2014; Seidel et al. 2008; Lu et al. 2007; Hu and Fu 2007), corresponding to the widening of the Hadley cells. However, this drying tendency cannot be found at all longitudes and is not pronounced enough to be clearly visible in the contour lines. Repeating the experiment with different threshold values (not shown) did not lead to clearer changes in the contour line.

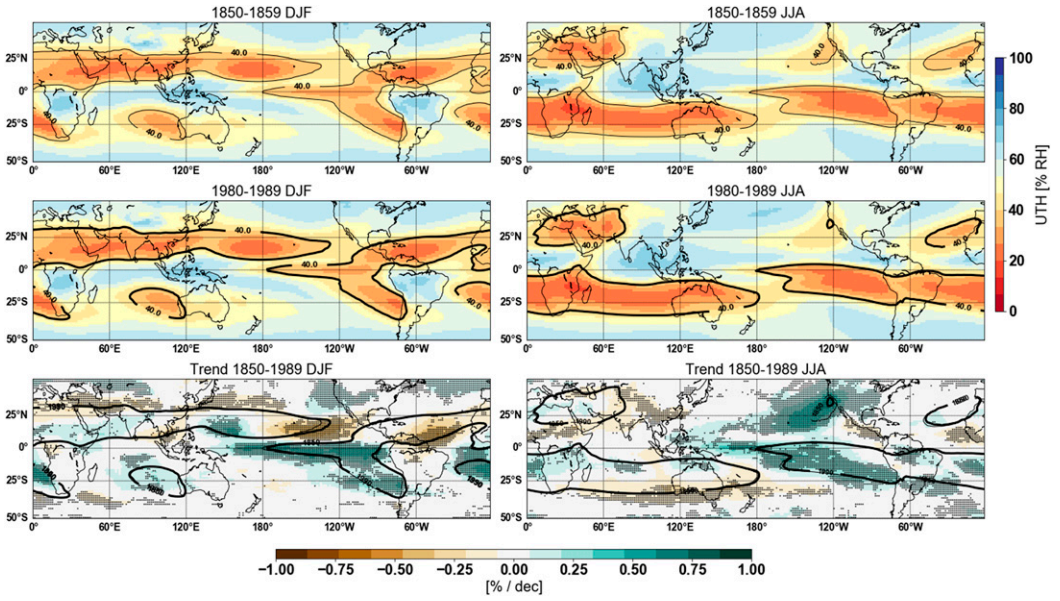

FIG. 2. As in Fig. 1, but calculated from the output of the historical simulation. Note the different scale than in Fig. 1.

Second, dry zones in the summer hemisphere are concentrated in the eastern ocean basins, where the descent zones of the subtropical anticyclones can be found. These atmospheric structures are centered in the lower levels of the troposphere and strongly influence moisture transport (Li et al. 2012). The mechanisms that underlie the development of subtropical anticyclones have been thoroughly studied in the last 20 years (He et al. 2017; Rodwell and Hoskins 2001; Seager et al. 2003; Miyasaka and Nakamura 2005, 2010). In summer these structures of the general circulation extend over the summer-hemispheric oceans and feature strong meridional equatorward flow on their eastern flanks, accompanied by strong subsidence (Seager et al. 2003). Miyasaka and Nakamura (2005, 2010) demonstrated that the formation of subtropical anticyclones and the associated descent is primarily driven by a zonally asymmetric diabatic heating pattern between land and ocean. This local land–sea contrast consists in low sea surface temperatures due to cold oceanic upwelling and radiative cooling over the eastern ocean basins, associated with marine stratus, and continental heating through sensible heat flux over the dry, heated landmass to the east.

In the UTH distribution of the CMIP5 ensemble mean, these regions in the eastern ocean basins in summer are characterized by low UTH (Fig. 1). After quadrupling of the CO_2 concentration (1980–89), UTH is increasing in the dry zones, most of all in the North Pacific and South Atlantic Oceans, except for the one over the eastern Mediterranean Sea region and the Middle East, where the dry zone presents signs of drying in the north and moistening in the south (Fig. 1, bottom panels). The signal of increasing UTH inside all the other dry regions is robust.

However, the 1pctCO2 simulations uses a strong forcing, and the increase in CO_2 is larger than the current increase in the real climate. These results give some indication about the evolution of UTH and the upper-tropospheric dry zones due to increased CO_2 concentration, but to have a more realistic view of UTH in climate change, we have looked at the climate simulations of the recent past, using the historical run of CMIP5 models. As expected, the changes in UTH in the 140 years of the historical experiment are smaller than in the idealized simulations (Fig. 2, bottom, as compared with Fig. 1, bottom). The extent of the dry zones, indicated by the black contour lines, hardly changes between the two decades. Nevertheless, a small drying tendency appears at the poleward edge of the winter dry zones over the Eurasian continent and the west Pacific, as well as over the Indian Ocean and Australia. Furthermore, UTH increases in several regions, but only the moistening trends of the descent regions in the North and South Pacific as well as in the South Atlantic (in summer seasons) are robust. In the northern subtropical Atlantic and northeast Pacific, UTH shows a decreasing signal in DJF through a majority of CMIP5 models. In all other regions where UTH is smaller than 40%, the models do not show any robust sign of change.

The forcings of the historical experiment are closer to the real atmosphere than those from the 1pctCO2 simulations. Still, satellite observations reflect many factors such as forcings associated with aerosols, volcanic activities, or land-use change. Not all of them are accurately

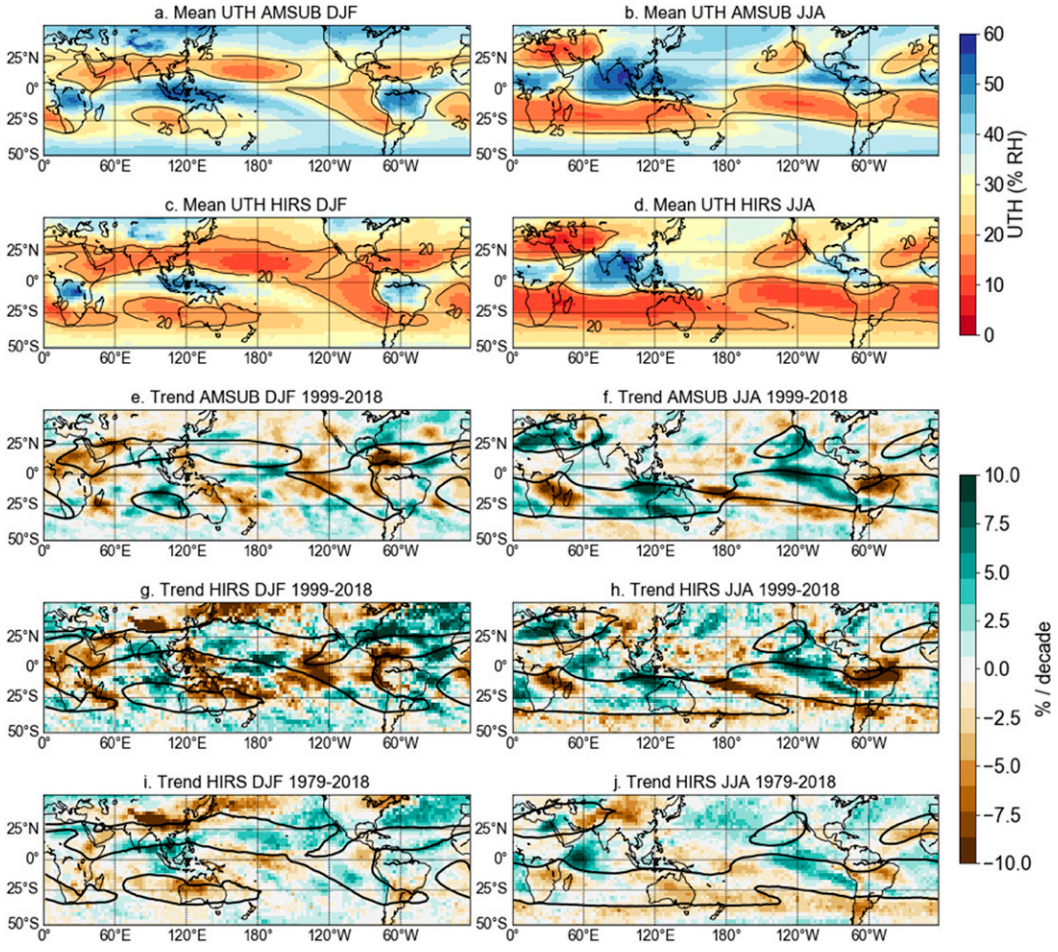

FIG. 3. For (left) boreal winter (DJF) and (right) boreal summer (JJA), mean of UTH from 1999 to 2018 from measurements with (a),(b) a microwave sensor (AMSU-B) and (c),(d) an infrared sensor (HIRS), trend of UTH for 1999–2018 from measurement with (e),(f) a microwave sensor (AMSU-B) and (g),(h) an infrared sensor (HIRS), and (i),(j) trend of UTH for 1979–2018 from measurement with an infrared sensor (HIRS). The black contour lines indicate the outline of the dry zones, where the mean of UTH $< 25\%$ RH for microwave and UTH $< 20\%$ RH for infrared. Note the different color scales than in Figs. 1 and 2. The trends are relative to the mean UTH of the period.

represented in models. Keeping the previous results in mind, we will analyze UTH from satellite observations to see whether some of the features that have appeared in the model data can be found in the satellite data.

b. *Trends from observations*

Figures 3a–d show the mean of UTH in DJF and JJA for the period from 1999 to 2018 calculated from satellite-based measurements with the microwave sensor (Figs. 3a,b) and the infrared sensor (Figs. 3c,d). UTH from brightness temperatures measured with the infrared sensor (HIRS) has been corrected using the reference pressure p_0 (cf. Soden and Bretherton 1993) to make it comparable to the microwave data. Nevertheless, UTH from infrared is lower than UTH from microwave measurements. But both distributions show the same seasonal pattern, which corresponds to the climatology described in previous studies (e.g., Gettelman et al. 2006; Bates and Jackson 2001). In both hemispheres a dry belt spreads over all longitudes in winter. Dry zones in the summer hemisphere are similar to the ones found in the model data.

However, UTH appears to be lower in observational than in the model data. While the dry zones in CMIP5 ensemble are bounded by the 40% RH contour line, the same regions are characterized by UTH of 25% and less in the microwave and infrared datasets from satellite-based measurements.

Also, unlike the models suggested, the decadal trends in UTH from 1999 to 2018 from microwave measurements (Figs. 3e,f) show no general tendency for drying at the poleward edge of the winter dry zones. Nor is there any consistent trend visible in the summer-hemispheric

dry zones in the eastern ocean basins. Because the observation period for microwave data is still short, we decided to compare the trend in UTH from microwave measurements with the one from infrared measurements, where UTH has been again corrected with the reference pressure. To make the trends for the two datasets better comparable, the plots show the decadal trends relative to the mean UTH shown in Figs. 3a–d. The pattern of trends in UTH from infrared brightness temperatures from 1999 to 2018 (Figs. 3g,h) is very similar to the pattern in UTH from microwave measurements. The main differences arise probably from the different spatial resolutions between the sensors [2.5° for infrared (Shi and Bates 2011) and 1.5° for microwave (Chung et al. 2013)]. Nevertheless, the trend in UTH from HIRS shows a drying signal at the poleward edge of the dry belt in JJA, which is not as clear in the microwave data.

Measurements from the infrared sensor HIRS have started in 1979, making it possible to analyze UTH for a period of 40 years. Because of the good agreement between the trends in UTH from both sensors for the common period (1999–2018), we assume that UTH from infrared measurements with the reference pressure can be used to analyze the trend for the longer period starting in 1979. The decadal trend in UTH from 1979 to 2018 does not show any consistent tendency for the summer-hemispheric dry zones in the eastern ocean basins. However, there is again a small drying trend at the poleward edge of the winter dry belt in the Southern Hemisphere as well as over parts of the Northern Hemisphere (Asia and the western Pacific) (Figs. 3g,h).

Notable is the difference in magnitude of the trends in UTH from satellite observations in comparison with UTH from CMIP5 model data (Figs. 1 and 2). The trends are given relative to the mean UTH distribution which is lower for the satellite data than for the model data. This could explain why the magnitude in trends is higher in the observational data, but the difference in magnitudes persists when considering the absolute trend values (not shown here). An explanation for this difference in range is that for the satellite data the time period is shorter, so that variability has more influence on the trend. The range of the trends in UTH from the longer infrared time series is already smaller than the ones from Figs. 3e–h. Trends from model data, on the other hand, are sampled in the ensemble mean of 25 different models. Each of these models taken alone would also show higher magnitudes in its UTH trends, which are leveled out in the ensemble mean.

Not only is the spatial distribution of the dry zones relevant for the climate, but the change in the global fraction of regions with low UTH matters as well, especially for the net radiation balance. Figure 4 shows the deseasonalized anomaly time series of the fraction of grid points with UTH below a given threshold. For the model data (historical run; microwave) dry zones are represented by the fraction of grid points where UTH is smaller than 40% (Fig. 4, top). For observations, the dry zones are defined by the fraction of grid points where UTH is smaller than 25% (microwave) and 20% (infrared) (Fig. 4, bottom). Due to different measuring periods of the satellite-based sensors, the time series of UTH from infrared radiances starts in 1979 (blue) and from microwave radiances in 1999 (red). In both datasets we excluded higher latitudes, because the different grid size would bias the results, but also because we are mainly interested in dry zones in the subtropics. We defined the dry zones in analogy to Roca et al. (2012) and Schröder et al. (2014), who introduced the frequency of occurrence of dry air as a marker of the behavior of the dry part of the UTH distribution. The different thresholds (25%, 30%, and 40%) reflect shifted distributions of UTH depending on the sensor and data sources. These thresholds nevertheless represent approximately the level of the 25th percentile of each distribution (the 25th percentile is illustrated in Fig. 5).

For the period when the observational data were available from both, HIRS and AMSU-B (1999–2018), the variation correlates well between both sensors (Fig. 4, bottom). However, the time series of the fraction of grid points with low UTH show different trends depending on the sensor used. While the fraction of grid points below the given threshold increases in both periods in the infrared dataset (+0.40% per decade for 1999–2018; +0.49% per decade for 1979–99), the same fraction slightly decreases for the microwave data in observations (−0.18% per decade) and CMIP5 ensemble mean (−0.02% per decade).

Hence, on a global view it is difficult to draw conclusions concerning the evolution of the area of upper-tropospheric dry zones. Furthermore, even for the infrared data the period is short enough that variability is important. The trends in UTH dry zones still differ between microwave and infrared data, despite the fact that the infrared data have been corrected with the reference pressure. Possible explanations will be discussed in the next section.

4. Discussion and conclusions

a. Discussion

We have analyzed UTH computed with a satellite simulation software from CMIP5 model data using an algorithm for a microwave sensor (AMSU-B) and compared it with UTH calculated from observational data for a microwave and an infrared sensor. Through the results shown in section 3, it has become clear that UTH, as calculated from radiance, cannot be analyzed

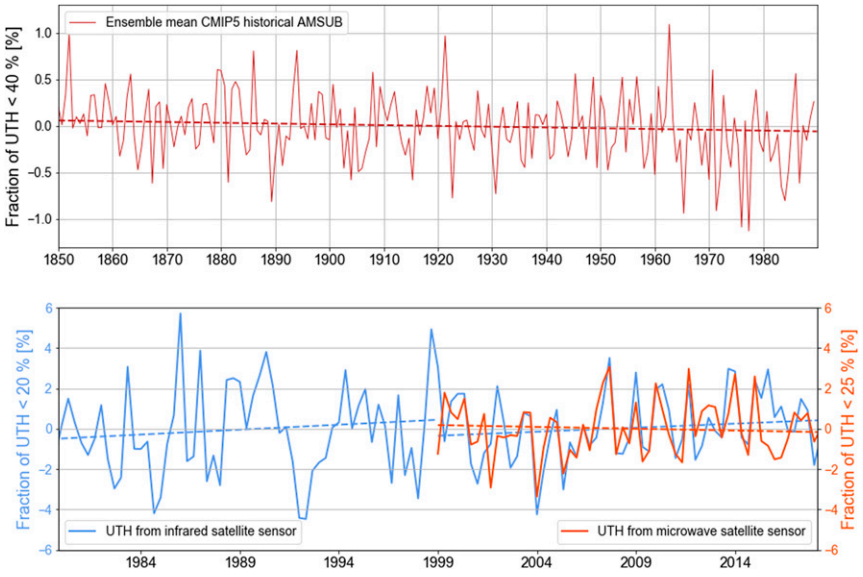

FIG. 4. (top) Deseasonalized and smoothed time series and linear trend of the fraction of grid points with UTH < 40% RH between 45°S and 45°N in CMIP5 models' historical run, computed for microwave sensor characteristics. (bottom) Deseasonalized and smoothed time series and linear trend of the fraction of grid points with UTH < 20% RH from observations with the infrared sensor (HIRS; blue) from 1979 to 2018 and of fraction of grid points with UTH < 25% RH from observations with the microwave sensor (AMSU-B; coral). The trend lines indicate linear trends in fraction of grid points with UTH smaller than the given threshold for the periods 1979–99 and 1999–2018 separately in infrared (blue) and for 1999–2018 in microwave (red). Note the different scales of the *y* axis for the top and bottom plots.

without taking into account the instrument used to retrieve the data. Not only is there a shift in the range of UTH between the dataset computed from model data and the one computed from observations, but a difference has been found in particular between the infrared and the microwave measuring method.

The distribution of UTH depending on the source reveals that, for both sensors, the simulations overestimate UTH in the tropics and subtropics compared to observations (Fig. 5). For completeness Fig. 5 also includes UTH from the CMIP5 ensemble calculated with the characteristics of the infrared sensor (Fig. 5, top right), but as UTH from model data has not been calculated using the reference pressure, this dataset has not further been used in the rest of the study. UTH from observations is concentrated in the range between 0% and 60% RH for the infrared sensor. For UTH from observations with a microwave sensor the shape of the distribution is very similar to UTH from simulations, but with a maximum around 30% RH as compared with 60% RH in the simulations. Because of the different calculation methods, UTH from the infrared instrument cannot be compared directly between model and observations. However, the distribution of UTH from infrared measurements (Fig. 5, bottom right) with the use of p_0 is similar to the distribution of UTH from microwave measurements.

Hence, UTH from infrared radiances is comparable to UTH from microwave radiances, if the reference pressure p_0 is used for the calculation. Lang (2019) found an explanation for this behavior. Indeed, different absorption characteristics of infrared and microwave UTH channels lead to stronger increase in brightness temperature from infrared radiances in a warming climate. When the atmosphere becomes warmer, the emission layer shifts to higher altitudes, where relative humidity and atmospheric pressure are smaller, which influences the measurement of brightness temperatures differently for infrared and microwave radiances. For comparison, Lang (2019) defined "real" UTH as the relative humidity averaged over an atmospheric layer bounded by two altitudes, both defined by fixed thresholds of integrated water vapor above. She found that UTH calculated from microwave radiances was closer to this so-called real UTH, whereas UTH from infrared radiances was subject to an artificial bias. This bias can be counterbalanced by the use of p_0.

Nevertheless, UTH from infrared measurements is still drier than UTH from microwave measurements, as we have seen in Fig. 4. The clear-sky sampling bias of the

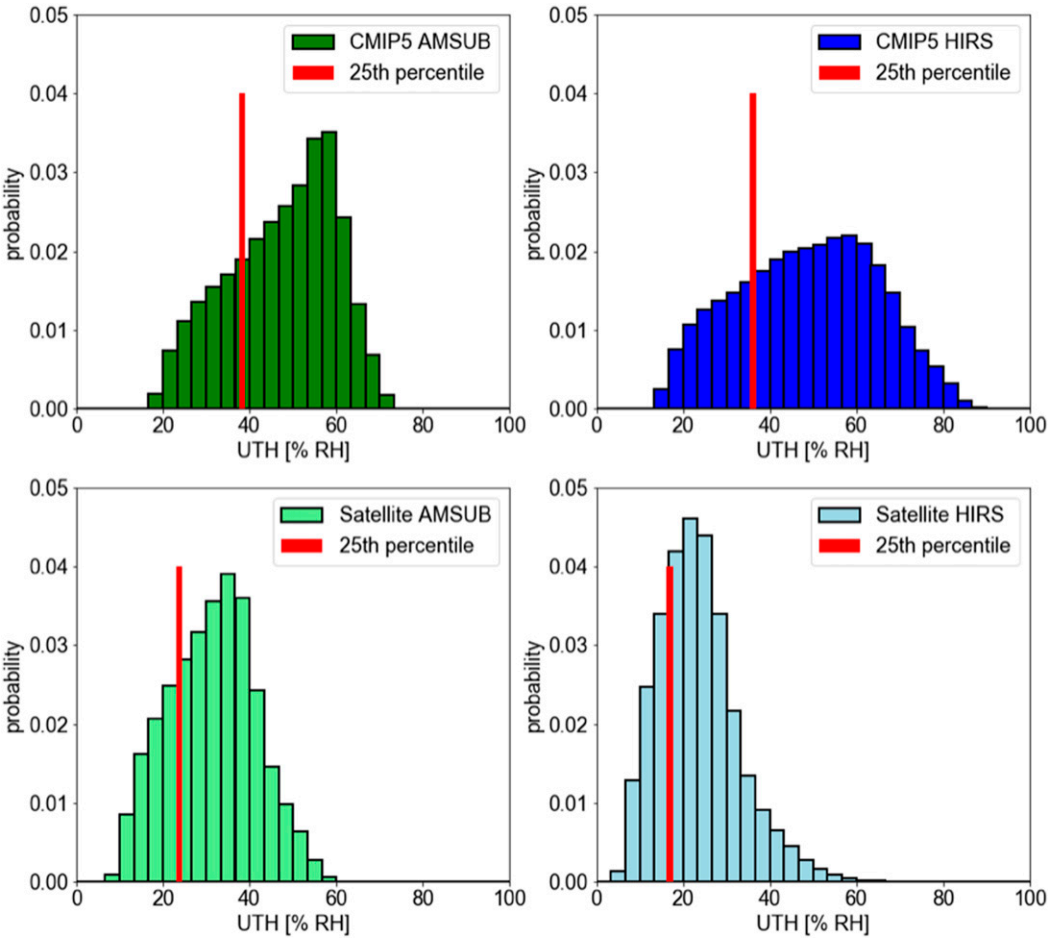

FIG. 5. Histograms of (top) the distribution of UTH from the first 30 years of the ensemble mean of the historical simulation with CMIP5 models for computation with (left) microwave and (right) infrared coefficients, and (bottom) the distribution of UTH from (left) microwave and (right) infrared observations, for all monthly means for each grid point between 45°S and 45°N.

observations can explain part of these differences, as discussed in section 2b. John et al. (2011) estimated that in the tropical mean this bias can account for roughly 7% of the infrared dry bias relative to microwave data and perhaps for a few percent dry bias of microwave data relative to the true all-sky mean. But even taking this into account, the CMIP5 ensemble is significantly wetter than the observations. This is consistent with the finding of John and Soden (2007) that CMIP models have a large moist bias in the free troposphere. Their study was based on CMIP3, but our analysis indicates that this is still true for CMIP5.

Considering the evolution of dry zones in climate change, the data support only a few robust conclusions. While previous studies suggest a poleward expansion of the subtropical subsidence zones (Birner et al. 2014; Seidel et al. 2008; Lu et al. 2007; Hu and Fu 2007; Hudson et al. 2006), the dry zones in the UTH distribution estimated from CMIP5 model output do not generally expand, even though there is a robust drying tendency in parts of the regions poleward of these dry belts in the winter hemisphere. Dry zones in the eastern Pacific even decrease in both seasons, however. In observations, the drying tendency can only be found in the Southern Hemisphere winter distribution in infrared data. Even more uncertain is the evolution of the dry zones situated in the summer hemisphere and corresponding to the subsidence regions of the subtropical anticyclones. There is a tendency toward increasing UTH in these regions, but this trend is robust in the model data only for the South Atlantic and South and North Pacific on the long term, and so far not supported by the observations. UTH may be sensitive to other factors, such as sea surface temperature changes, which could explain different signals in the South Pacific. Other studies also state a weakening and westward shift of the Walker circulation, which could be

another factor influencing the dry zones in the eastern South Pacific (e.g., Vecchi and Soden 2007).

The results from our model analysis overlap with the recent study of He et al. (2017), where the multimodel output from CMIP5 simulations was used to investigate the response of subtropical anticyclones to global warming by analyzing subsidence, low-level divergence, and rotational wind. They found that the subtropical anticyclones over the North Pacific, South Atlantic, and south Indian Ocean are projected to become weaker, while the North Atlantic subtropical anticyclone intensifies. These results correspond to our findings of increasing UTH in the dry zones of the eastern North Pacific and South Atlantic in the CMIP5 ensemble for the 1pctCO2 and the historical simulations (Figs. 1 and 2). But from our simulations, the trends of He et al. (2017) cannot be confirmed for the south Indian Ocean and the eastern North Atlantic, and we also found a robust signal of increasing UTH in the South Pacific. Finally, none of the trends for the subtropical anticyclones could be found in UTH from observations. The complexity of the subtropical anticyclones in their respective climatic environment makes it difficult to make a general statement concerning the evolution of the corresponding upper-tropospheric dry zones. It would be interesting to analyze each of them separately and understand more about the mechanisms behind these structures.

b. *Conclusions and outlook*

Increasing atmospheric CO_2 concentration impacts the distribution of upper-tropospheric humidity and in particular the extension of the subtropical dry zones. UTH has been calculated from model data with a satellite simulation software using the characteristics of a microwave sensor. The results have shown that upper-tropospheric dry zones form a belt in the winter hemisphere and that in an experiment with yearly 1% increasing CO_2 concentration, there appears a drying tendency at the poleward edge of this dry belt over large parts of the globe. In historical simulations this drying trend is not as pronounced, but is still visible. Nevertheless, and, despite these drying tendencies, no clear poleward shift or expansion of the dry belts can be found in this dataset. In the summer hemisphere, the dry zones are concentrated in the eastern ocean basins, and correspond to the descent regions of the subtropical anticyclones. In these regions, UTH from CMIP5 ensemble evaluated from the microwave perspective increases in the South Atlantic and the North and South Pacific, reflecting a weakening of the anticyclones, at least partially in agreement with the study by He et al. (2017).

Observational data from infrared and microwave sensors have been used to investigate the evolution of upper-tropospheric dry zones since 1979. The general seasonal pattern conforms to the one found in the model data. UTH calculated from brightness temperatures measured from an infrared sensor shows the drying tendency at the poleward edge of the winter dry belt even for the shorter time scale. But this drying does not indicate a clear expansion of the winter dry belt and has not been found for UTH from microwave measurements. Finally, no robust trend could be detected for the summer dry zones.

The reasons for the different results concerning summer dry zones can probably be found in the complex mechanisms behind the subtropical anticyclones. While the change of tropical circulation structures like the Hadley cell or the Walker circulation have been studied extensively in the last 50 years, subtropical anticyclones have only recently gotten more attention (e.g., Rodwell and Hoskins 2001; Miyasaka and Nakamura 2005, 2010; He et al. 2017). Their behavior with global warming is still an interesting subject of study. To further investigate the evolution of upper-tropospheric dry zones, it may be necessary to gain a better understanding and achieve more robust simulations of subtropical anticyclones.

Acknowledgments. We acknowledge the World Climate Research Programme's Working Group on Coupled Modelling, which is responsible for CMIP, and we thank the climate modeling groups (listed in Table 1 of this paper) for producing and making available their model output. For CMIP the U.S. Department of Energy's Program for Climate Model Diagnosis and Intercomparison provides coordinating support and led development of software infrastructure in partnership with the Global Organization for Earth System Science Portals. We are grateful to the developers of the RTTOV software packages that we used to simulate satellite observations from model data. With this work we contribute to the Cluster of Excellence ''CLICCS—Climate, Climatic Change, and Society'' contribution to the Center for Earth System Research and Sustainability (CEN) of Universität Hamburg. We are grateful for fruitful discussions within the EU H2020 project FIDUCEO (Grant Agreement 638822) and also thank Theresa Lang and Laura Dietrich for enlightening discussions about the calculation of UTH. We also gratefully acknowledge the constructive feedback from editor Dr. Karen Shell and three anonymous reviewers. Special thanks are given to Dr. Andreas Oschlies from the GEOMAR Helmholtz Centre for Ocean Research Kiel, where this work was partly performed.

REFERENCES

Bates, J. J., and D. L. Jackson, 2001: Trends in upper tropospheric humidity. *Geophys. Res. Lett.*, **28**, 1695–1698, https://doi.org/10.1029/2000GL012544.

Birner, T., S. M. Davis, and D. J. Seidel, 2014: The changing width of Earth's tropical belt. *Phys. Today*, **67**, 38–44, https://doi.org/10.1063/PT.3.2620.

Buehler, S. A., and V. O. John, 2005: A simple method to relate microwave radiances to upper troposphere humidity. *J. Geophys. Res.*, **110**, D02110, https://doi.org/10.1029/2004JD005111.

Cai, W., T. Cowan, and M. Thatcher, 2012: Rainfall reductions over Southern Hemisphere semi-arid regions: The role of subtropical dry zone expansion. *Sci. Rep.*, **2**, 702, https://doi.org/10.1038/srep00702.

Chung, E.-S., B. J. Soden, and V. O. John, 2013: Intercalibrating microwave satellite observations for monitoring long-term variations in upper- and midtropospheric water vapor. *J. Atmos. Oceanic Technol.*, **30**, 2303–2319, https://doi.org/10.1175/JTECH-D-13-00001.1.

Gettelman, A., W. D. Collins, E. J. Fetzer, A. Eldering, F. W. Irion, P. B. Duffy, and G. Bala, 2006: Climatology of upper-tropospheric relative humidity from the Atmospheric Infrared Sounder and implications for climate. *J. Climate*, **19**, 6104–6121, https://doi.org/10.1175/JCLI3956.1.

Gierens, K., K. Eleftheratos, and L. Shi, 2014: Technical note: 30 years of HIRS data of upper tropospheric humidity. *Atmos. Chem. Phys.*, **14**, 7533–7541, https://doi.org/10.5194/acp-14-7533-2014.

He, C., B. Wu, L. Zou, and T. Zhou, 2017: Responses of the summertime subtropical anticyclones to global warming. *J. Climate*, **30**, 6465–6479, https://doi.org/10.1175/JCLI-D-16-0529.1.

Held, I. M., and B. J. Soden, 2000: Water vapor feedback and global warming. *Annu. Rev. Energy Environ.*, **25**, 441–475, https://doi.org/10.1146/annurev.energy.25.1.441.

Hu, Y., and Q. Fu, 2007: Observed poleward expansion of the Hadley circulation since 1979. *Atmos. Chem. Phys.*, **7**, 5229–5236, https://doi.org/10.5194/acp-7-5229-2007.

Hudson, R., M. Andrade, M. Follette, and A. Frolov, 2006: The total ozone field separated into meteorological regimes–Part II: Northern Hemisphere mid-latitude total ozone trends. *Atmos. Chem. Phys.*, **6**, 5183–5191, https://doi.org/10.5194/acp-6-5183-2006.

Jackson, D. L., and J. J. Bates, 2001: Upper tropospheric humidity algorithm assessment. *J. Geophys. Res.*, **106**, 32 259–32 270, https://doi.org/10.1029/2001JD000348.

——, D. P. Wylie, and J. J. Bates, 2003: The HIRS Pathfinder Radiance data set (1979–2001). *12th Conf. on Satellite Meteorology and Oceanography*, Long Beach, CA, Amer. Meteor. Soc., P1.8, https://ams.confex.com/ams/pdfpapers/57094.pdf.

Johanson, C. M., and Q. Fu, 2009: Hadley cell widening: Model simulations versus observations. *J. Climate*, **22**, 2713–2725, https://doi.org/10.1175/2008JCLI2620.1.

John, V. O., and B. J. Soden, 2007: Temperature and humidity biases in global climate models and their impact on climate feedbacks. *Geophys. Res. Lett.*, **34**, L18704, https://doi.org/10.1029/2007GL030429.

——, G. Holl, R. P. Allan, S. A. Buehler, D. E. Parker, and B. J. Soden, 2011: Clear-sky biases in satellite infrared estimates of upper tropospheric humidity and its trends. *J. Geophys. Res.*, **116**, D14108, https://doi.org/10.1029/2010JD015355.

Lang, T., 2019: A new climate data record of upper tropospheric humidity. M.S. thesis, Meteorological Institute, Universität Hamburg, 117 pp, https://arts.mi.uni-hamburg.de//publications/grouppapers2/lang19_new_msc.pdf.

Lau, W. K. M., and K.-M. Kim, 2015: Robust Hadley circulation changes and increasing global dryness due to CO_2 warming from CMIP5 model projections. *Proc. Natl. Acad. Sci. USA*, **112**, 3630–3635, https://doi.org/10.1073/pnas.1418682112.

Li, W., L. Li, M. Ting, and Y. Liu, 2012: Intensification of Northern Hemisphere subtropical highs in a warming climate. *Nat. Geosci.*, **5**, 830–834, https://doi.org/10.1038/ngeo1590.

Lu, J., G. A. Vecchi, and T. Reichler, 2007: Expansion of the Hadley cell under global warming. *Geophys. Res. Lett.*, **34**, L06805, https://doi.org/10.1029/2006GL028443.

Miyasaka, T., and H. Nakamura, 2005: Structure and formation mechanisms of the Northern Hemisphere summertime subtropical highs. *J. Climate*, **18**, 5046–5065, https://doi.org/10.1175/JCLI3599.1.

——, and ——, 2010: Structure and mechanisms of the Southern Hemisphere summertime subtropical anticyclones. *J. Climate*, **23**, 2115–2130, https://doi.org/10.1175/2009JCLI3008.1.

Pierrehumbert, R. T., 1995: Thermostats, radiator fins, and the local runaway greenhouse. *J. Atmos. Sci.*, **52**, 1784–1806, https://doi.org/10.1175/1520-0469(1995)052<1784:TRFATL>2.0.CO;2.

Roca, R., R. Guzman, J. Lemond, J. Meijers, L. Picon, and H. Brogniez, 2012: Tropical and extra-tropical influences on the distribution of free tropospheric humidity over the inter-tropical belt. *Surv. Geophys.*, **33**, 565–583, https://doi.org/10.1007/s10712-011-9169-4.

Rodwell, M. J., and B. J. Hoskins, 2001: Subtropical anticyclones and summer monsoons. *J. Climate*, **14**, 3192–3211, https://doi.org/10.1175/1520-0442(2001)014<3192:SAASM>2.0.CO;2.

Saunders, R. W., M. Matricardi, and A. Geer, 2010: RTTOV-9 users guide, version 1.7. EUMETSAT Satellite Application Facility on Numerical Weather Prediction Tech. Rep. NWPSAF-MO-UD-016, 57 pp., https://nwpsaf.eu/oldsite/deliverables/rtm/rttov9_files/users_guide_9_v1.7.pdf.

Scheff, J., and M. W. Frierson, 2012: Robust futures precipitation declines in CMIP5 largely reflect the poleward expansion of model subtropical dry zones. *Geophys. Res. Lett.*, **39**, L18704, https://doi.org/10.1029/2012GL052910.

Schröder, M., R. Roca, A. Kniffka, and H. Brogniez, 2014: Climatology of free-tropospheric humidity: Extension into the SEVIRI era, evaluation and exemplary analysis. *Atmos. Chem. Phys.*, **14**, 11 129–11 148, https://doi.org/10.5194/acp-14-11129-2014.

Schulzweida, U., 2019: CDO user guide, 215 pp., https://doi.org/10.5281/zenodo.2558193.

Seager, R., R. Murtugudde, N. Naik, A. Clement, N. Gordon, and J. Miller, 2003: Air–sea interaction and the seasonal cycle of the subtropical anticyclones. *J. Climate*, **16**, 1948–1966, https://doi.org/10.1175/1520-0442(2003)016<1948:AIATSC>2.0.CO;2.

Seidel, D. J., Q. Fu, W. J. Randel, and T. J. Reichler, 2008: Widening of the tropical belt in a changing climate. *Nat. Geosci.*, **1**, 21–24, https://doi.org/10.1038/ngeo.2007.38.

Sherwood, S. C., W. Ingram, Y. Tsushima, M. Satoh, M. Roberts, P. L. Vidale, and P. O'Gorman, 2010: Relative humidity changes in a warmer climate. *J. Geophys. Res.*, **115**, D09104, https://doi.org/10.1029/2009JD012585.

Shi, L., and J. J. Bates, 2011: Three decades of intersatellite-calibrated High-Resolution Infrared Radiation Sounder upper tropospheric water vapor. *J. Geophys. Res.*, **116**, D04108, https://doi.org/10.1029/2010JD014847.

——, ——, and C. Cao, 2008: Scene radiance–dependent intersatellite biases of HIRS longwave channels. *J. Atmos.*

Oceanic Technol., **25**, 2219–2229, https://doi.org/10.1175/2008JTECHA1058.1.

Soden, B. J., and F. P. Bretherton, 1993: Upper tropospheric relative humidity from the GEOS 6.7 μm channel: Method and climatology for July 1987. *J. Geophys. Res.*, **98**, 16 669–16 688, https://doi.org/10.1029/93JD01283.

Spencer, R. W., and D. Braswell, 1997: How dry is the tropical free troposphere? Implication for global warming theory. *Bull. Amer. Meteor. Soc.*, **78**, 1097–1106, https://doi.org/10.1175/1520-0477(1997)078<1097:HDITTF>2.0.CO;2.

Stephens, G. L., D. L. Jackson, and I. Wittmeyer, 1996: Global observations of upper-tropospheric water vapor derived from TOVS radiance data. *J. Climate*, **9**, 305–326, https://doi.org/10.1175/1520-0442(1996)009<0305:GOOUTW>2.0.CO;2.

Taylor, K. E., R. J. Stouffer, and G. A. Meehl, 2012: An overview of CMIP5 and the experiment design. *Bull. Amer. Meteor. Soc.*, **93**, 485–498, https://doi.org/10.1175/BAMS-D-11-00094.1.

Vecchi, G. A., and B. J. Soden, 2007: Global warming and the weakening of the tropical circulation. *J. Climate*, **20**, 4316–4340, https://doi.org/10.1175/JCLI4258.1.